J Appl Electrochem (2009) 39:2433–2438
DOI 10.1007/s10800-009-9931-1

ORIGINAL PAPER

Preparation and electrochemical properties of spherical $LiFePO_4$ and $LiFe_{0.9}Mg_{0.1}PO_4$ cathode materials for lithium rechargeable batteries

Zhaolin Liu · Xinhui Zhang · Liang Hong

Received: 23 March 2009 / Accepted: 7 May 2009 / Published online: 21 May 2009

Abstract The spherical $LiFePO_4$/C and $LiFe_{0.9}Mg_{0.1}PO_4$/C powders were successfully prepared from spherical $FePO_4$ via a simple uniform-phase precipitation method at normal pressure, using $FeCl_3$ and H_3PO_4 as the reactants. The $FePO_4$, $LiFePO_4$/C, and $LiFe_{0.9}Mg_{0.1}PO_4$/C powders were characterized by scanning electron microscopies (SEM), powder X-ray diffraction (XRD), X-ray photoelectron spectrometer (XPS), and tap-density testing. The uniform spherical particles produced are amorphous, but they were crystallized to $FePO_4$ after calcining above 400 °C. Due to the homogeneity of the basic $FePO_4$, the final products, $LiFePO_4$/C and $LiFe_{0.9}Mg_{0.1}PO_4$/C, are also significantly uniform and the particle size is of about 1 μm in diameter. The tap-density of the spherical $LiFePO_4$/C and $LiFe_{0.9}Mg_{0.1}PO_4$/C are 1.75 and 1.77 g cm^{-3}, respectively, which are remarkably higher than the non-spherical $LiFePO_4$ powders (the tap-density is 1.0–1.3 g cm^{-3}). The excellent specific capacities of 148 and 157 mAh g^{-1} with a rate of 0.1 C are achieved for the $LiFePO_4$/C and $LiFe_{0.9}Mg_{0.1}PO_4$/C, respectively. Comparison of the cyclic voltammograms of $LiFePO_4$/C and $LiFe_{0.9}Mg_{0.1}PO_4$/C shows enhanced redox current and reversibility for the sample substituting Mg on the Fe site. $LiFe_{0.9}Mg_{0.1}PO_4$/C exhibits better high-rate and cycle performances than the un-substituted $LiFePO_4$/C.

Keywords $LiFePO_4$ · $LiFe_{0.9}Mg_{0.1}PO_4$ · Spherical · High tap-density · Lithium batteries

Z. Liu (✉) · X. Zhang · L. Hong
Institute of Materials Research & Engineering, 3 Research Link, Singapore 117602, Singapore
e-mail: zl-liu@imre.a-star.edu.sg

1 Introduction

Phosphates $LiMPO_4$ (M = Mn, Fe, Co, or Ni) have been investigated intensively as promising cathode materials for lithium batteries [1–9]. Among this series of materials, $LiFePO_4$ is a low cost material and highly compatible to the environment. $LiFePO_4$ offers several advantages compared with $LiCoO_2$, $LiMn_2O_4$ and their derivatives. $LiFePO_4$ offers several advantages: (i) a relatively high theoretical specific capacity of 170 mAh g^{-1}, (ii) good reversibility of cathode reactions, (iii) high thermal and chemical stability, (iv) low material cost and toxicity, and (v) improved safety. In spite of these attractive features, $LiFePO_4$ requires further modifications to overcome limitations of poor electronic conductivity, which leads to initial capacity loss and poor rate capability, and the low pile density, which leads to low volumetric specific capacity.

Several researchers [10–13] explained synthesis of spherical powders could be an effective way to increase the tap-density and safety of the powder. The tap-density of $LiFePO_4$ powder is usually 1.0–1.3 g cm^{-3}, which is much lower than the tap-density of commercially used $LiCoO_2$ (2.3–2.5 g cm^{-3}). The low tap-density of $LiFePO_4$ limits the energy density of lithium ion batteries. The powders composed of spherical particles have higher density than the powders composed of irregular particles. Therefore, to obtain high tap-density of $LiFePO_4$ powder, preparing spherical powders is expected as an effective way.

Several papers have suggested metal ion doping as a method for improving performance [6, 14–16]. Substituting Mg and other species on the Li site was reported by Chung et al. [6] to give a greatly increase in conductivity of $LiFePO_4$ and a greatly improved electrode performance. The first reported work on substituting Mg on the Fe site

($LiFe_{1-x}Mg_xPO_4$ materials) was reported by Barker et al. [17] who successfully synthesized $LiFe_{0.9}Mg_{0.1}PO_4$ via a carbothermal reaction. Later several publications confirmed the formation of this material under different synthesis conditions and reported improved capacity, conductivity, and rate capability [18–21].

In this study, spherical $LiFePO_4$/C and $LiFe_{0.9}Mg_{0.1}PO_4$/C cathode materials were synthesized by a solid-mixture of Li_2CO_3, spherical $FePO_4$, and sugar. The physicochemical properties and electrochemical behaviors of the samples were characterized.

2 Experimental

Following the method reported by Wilhelmy and Matijević [22], spherical $FePO_4$ powder was prepared by aging a solution of $FeCl_3$ (2×10^{-3} M) and H_3PO_4 (3×10^{-2} M) at 40 °C. The resulting particles were thoroughly washed by distilled water and finally dried in vacuum at 60 °C for 24 h. The spherical $FePO_4 \cdot xH_2O$ powder was pre-heat treated at 550 °C for 7 h in air to obtain spherical anhydrous $FePO_4$ powder. For preparing spherical $LiFePO_4$/C and $LiFe_{0.9}Mg_{0.1}PO_4$/C, stoichiometric amounts of LiOH, $Mg(OH)_2$, and sugar were uniformly mixed in a molar ration of $LiOH:Mg(OH)_2:sugar:H_2O = 1.0:0.1:0.1:4$. Then, spherical $FePO_4$ powder in a molar ratio of $FePO_4:LiOH = 1:1$ was added into the slurry and agitated the mixture. The mixed slurry was dried and then heated at 600 °C for 5 h in Ar flow.

The sample morphology was examined by a JSM 6700 field emission scanning electron microscope (FESEM) operating at an accelerating voltage of 5 kV. The amount of carbon and Mg was determined by Oxford INCA Energy Dispersive X-ray (EDX) Spectrometer. The crystal structures of samples were characterized by X-ray diffraction (XRD) on a Bruker GADDS diffractometer using Cu Kα radiation and a graphite monochromator. The surface elements' content of $LiFePO_4$/C and $LiFe_{0.9}Mg_{0.1}PO_4$/C powders were determined by an X-ray photoelectron spectrometer (XPS, VG ESCALAB MKII) equipped with a Mg Kα X-ray sources.

The spherical $LiFePO_4$/C and $LiFe_{0.9}Mg_{0.1}PO_4$/C were mixed with 10 wt% of carbon black and 10 wt% of poly vinylidene difluoride (PVDF) in 1-methyl-2-pyrrolidinone (NMP). The slurry was used to coat 20-μm thick aluminium disks of 13 mm diameter to a mass loading of 2 mg cm^{-2} after drying (at 120 °C) and compaction (at 2.0×10^6 Pa). Each coated electrode was assembled in a 2,016 coin cell using a lithium counter electrode, a microporous polypropylene separator, and an electrolyte of 1 M $LiPF_6$ in a 50:50 (w/w) mixture of ethylene carbonate (EC) and diethyl carbonate (DEC). Cell assembly was carried out in an argon-filled glove box with less than 1 ppm each of oxygen and moisture.

The cells were discharged and charged at 25 °C on a Bitrode battery test system. Cyclic voltammetry was conducted with an EG&G model 263A potentiostat/galvonostat.

3 Results and discussion

The morphology for $FePO_4$, $LiFePO_4$/C, and $LiFe_{0.9}Mg_{0.1}PO_4$/C powders was observed on SEM, as shown in Fig. 1. The $FePO_4$ particles are small spherical particles that are fairly well-dispersed, and have a uniform particles size (about 1 μm) distribution (Fig. 1a). It is obviously recognized that the small spherical particles grow via the aggregation of small primary particles, similar to the case of spherical nickel [23], manganese [24], and iron [25] phosphate particles reported previously. The $LiFePO_4$/C and $LiFe_{0.9}Mg_{0.1}PO_4$/C particles are also composed of spherical particles similar to the $FePO_4$ precursors (Fig. 1b, c), although there are small quantities of fragments. The tap-density of the spherical $LiFePO_4$/C and $LiFe_{0.9}Mg_{0.1}PO_4$/C powders are 1.75 and 1.77 g cm^{-3}, respectively, which are remarkably higher than the non-spherical $LiFePO_4$ powders (the tap-density is 1.0–1.3 g cm^{-3}). For practical applications, the high tap-density of $LiFePO_4$ cathode materials leads to the high volumetric specific capacity.

The XRD spectra of $FePO_4$ after being treated at different temperatures are shown in Fig. 2. It can be seen obviously that the $FePO_4$ produced are amorphous. This amorphous structure strongly supports that the uniform spherical particles are agglomerates of primary particles as same as reported for iron phosphate particles [25]. The amorphous structure is preserved up to 300 °C. After calcining the particles above 400 °C, the characteristic XRD patterns of $FePO_4$ appear. In the present study, considerable crystallization has occurred under heating at 400 °C. Nevertheless, the crystalline peak intensities of the 400 °C samples are less than those samples prepared at higher temperatures. The crystallization temperature of $LiFePO_4$ has been reported to be ~567 °C, based on a different thermal analysis study [26]. The spectrum of $LiFe_{0.9}Mg_{0.1}PO_4$/C is almost the same as the spectrum of pure ordered orthorhombic olivine structured $LiFePO_4$ (Fig. 3). The absence of any other signals indicates there are no unwanted impurity phases, such as Li_3PO_4 and Fe^{3+} related compounds. No evidence of diffraction peaks for crystalline carbon appeared in the diffraction patterns, which indicates that the carbon generated from sugar is amorphous carbon and its presence does not influence the structure of $LiFePO_4$. The amounts of carbon in the

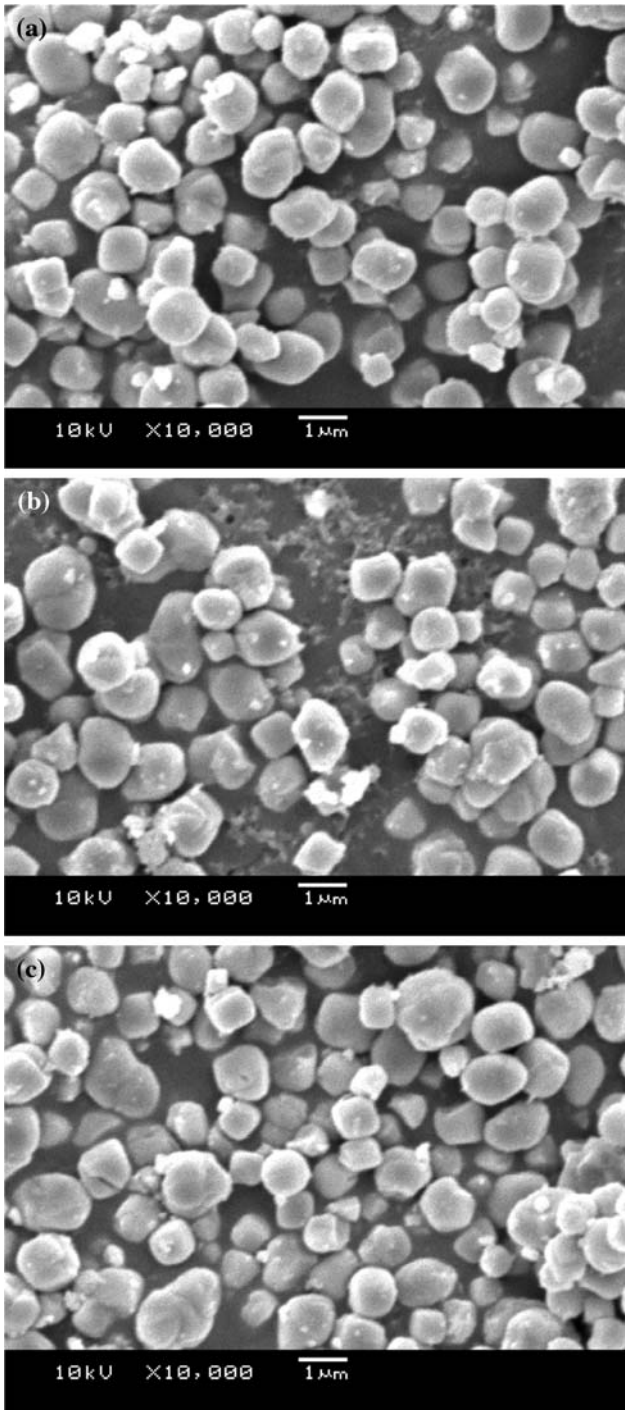

Fig. 1 SEM images of $FePO_4$ (**a**), $LiFePO_4$/C (**b**), and $LiFe_{0.9}Mg_{0.1}PO_4$/C (**c**) powders

$LiFePO_4$/C and $LiFe_{0.9}Mg_{0.1}PO_4$/C are about 8.15 and 8.28 wt%, respectively, through the element analysis, in other words, the molar ratios of $LiFePO_4$:C and $LiFe_{0.9}Mg_{0.1}PO_4$:C are about 1:1.17 and 1:1.19, respectively.

In order to examine the surface elements' content of the $LiFePO_4$/C and $LiFe_{0.9}Mg_{0.1}PO_4$/C, XPS analysis was performed. As shown in Fig. 4, a sharp peak at about

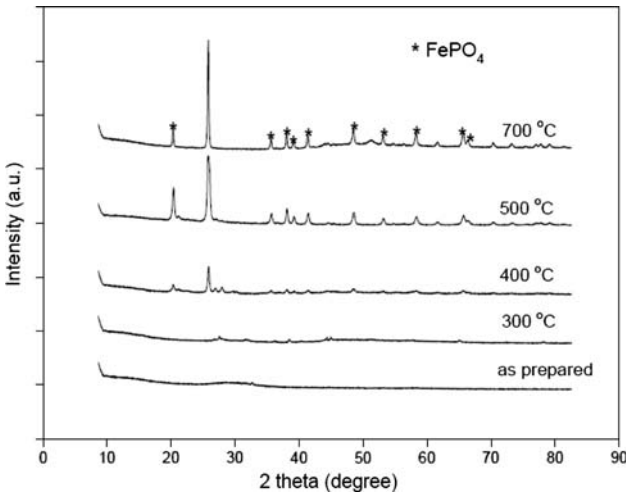

Fig. 2 XRD spectra of $FePO_4$ treated at different temperatures of 300, 400, 500, and 700 °C for 3 h in air

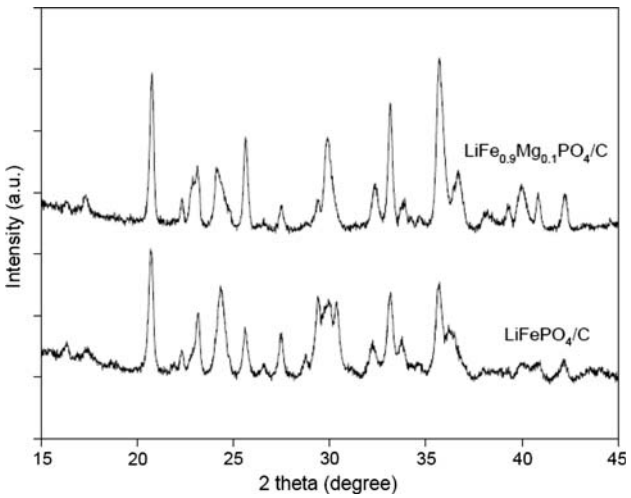

Fig. 3 XRD spectra of $LiFePO_4$/C and $LiFe_{0.9}Mg_{0.1}PO_4$/C prepared at 600 °C for 5 h in Ar flow

283.5 eV corresponding to C 1*s* with a high intensity is noted. The binding energy of Fe 2*p*, O 1*s*, and P 2*p* are determined to be 709.4, 529.5, and 131.5 eV, respectively. As the binding energy for the Li 1*s* emission peak at 55.6 eV is very close to the Fe 3*p* peak at about 54.1 eV, accurate determination of its binding energy and estimation of the element content were precluded. Mg 2*p* peak at 50.0 eV is not seen clearly since it is superposed on the Fe 3*p* and Li 1*s* at about 54.1 eV. According to XPS analysis on the surface of the $LiFePO_4$/C and $LiFe_{0.9}Mg_{0.1}PO_4$/C, the C:P molar ratios are about 6:1 and 5.9:1, which indicate the surface composition should be mainly the carbon and the $LiFePO_4$ or $LiFe_{0.9}Mg_{0.1}PO_4$ particles rather perfectly coated by carbon [12]. EDX spectra of the $LiFePO_4$/C and $LiFe_{0.9}Mg_{0.1}PO_4$/C are shown in Fig. 5. The Mg:Fe molar ratio is 1:8.6 in the $LiFe_{0.9}Mg_{0.1}PO_4$/C, which

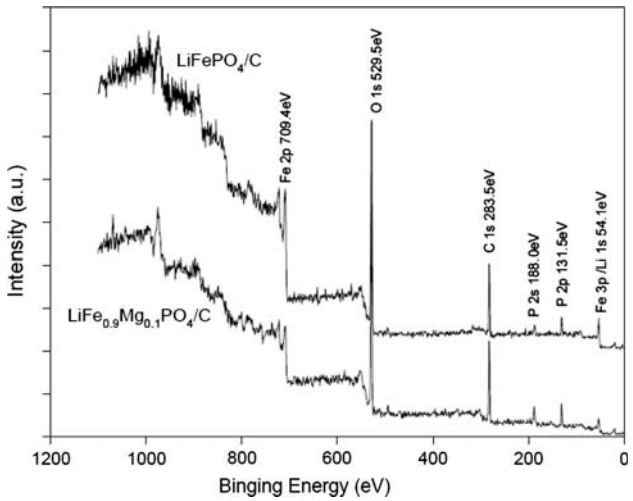

Fig. 4 XPS spectra of $LiFePO_4$/C and $LiFe_{0.9}Mg_{0.1}PO_4$/C powders

corresponded well with the amounts of Mg and Fe used in the starting mixture. The results of XPS and EDX analysis indicate that the Li, Fe, P, C, and Mg contents in the $LiFePO_4$/C and $LiFe_{0.9}Mg_{0.1}PO_4$/C are about the same as that in the initial mixtures.

Typical charge/discharge curves of the $LiFePO_4$/C in the first two cycles with low current density (0.1 C) are shown in Fig. 6. The first discharge capacity is 148 mAh g^{-1}, and then increases to 157 mAh g^{-1} in the second cycle, which is due to the "activation" of the first cycle reaction [27]. A flat and long voltage curve around 3.4 V indicates that the two-phase redox reaction proceeds via a first-order transition between $LiFePO_4$ and $FePO_4$. The large discharge capacity of the samples was due to the relatively small particle size. The electronic conductivity of $LiFePO_4$ is very low, and diffusion of Li^+ ion in the olivine structure is slow [1, 4, 28]. The smaller particle size, which is helpful for accessibility of the redox centers, is preferable to achieve larger capacity.

The results of CV experiments on $LiFePO_4$/C and $LiFe_{0.9}Mg_{0.1}PO_4$/C are presented in Fig. 7, where anodic and cathodic peaks appear at ~3.6 and 3.3 V for both materials, respectively. The main differences between $LiFePO_4$/C and $LiFe_{0.9}Mg_{0.1}PO_4$/C are in the peak shapes and heights of the voltammogram. The redox current for $LiFe_{0.9}Mg_{0.1}PO_4$/C (0.85 mA) is higher than that for $LiFePO_4$/C (0.68 mA). The larger redox current for $LiFe_{0.9}Mg_{0.1}PO_4$/C results from its higher utilization due to its good electronic conductivity and lithium ion diffusivity, compared with the un-doped $LiFePO_4$/C.

Figure 8 shows discharge curves of the $LiFePO_4$/C and $LiFe_{0.9}Mg_{0.1}PO_4$/C measured at various rates. The

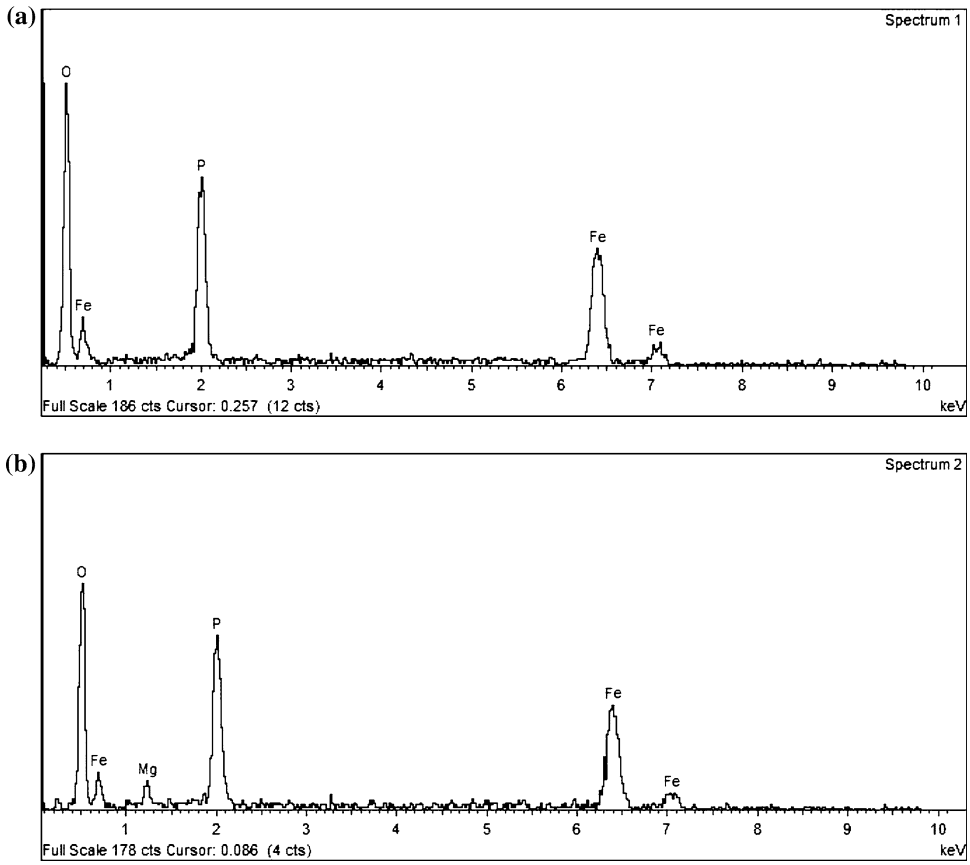

Fig. 5 EDX spectra of $LiFePO_4$/C (**a**) and $LiFe_{0.9}Mg_{0.1}PO_4$/C (**b**) powders

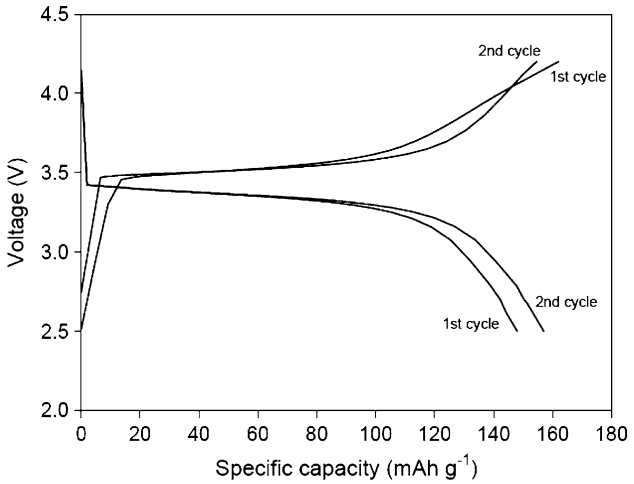

Fig. 6 Typical charge/discharge curves of $LiFePO_4$/C powder at 0.1 C

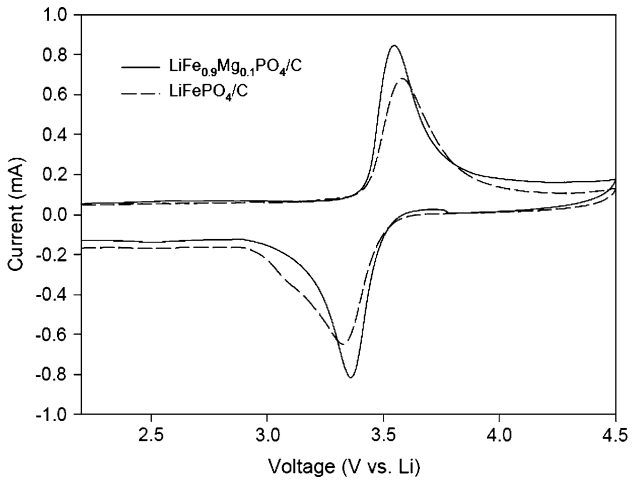

Fig. 7 Cyclic voltammograms of $LiFePO_4$/C and $LiFe_{0.9}Mg_{0.1}PO_4$/C powders

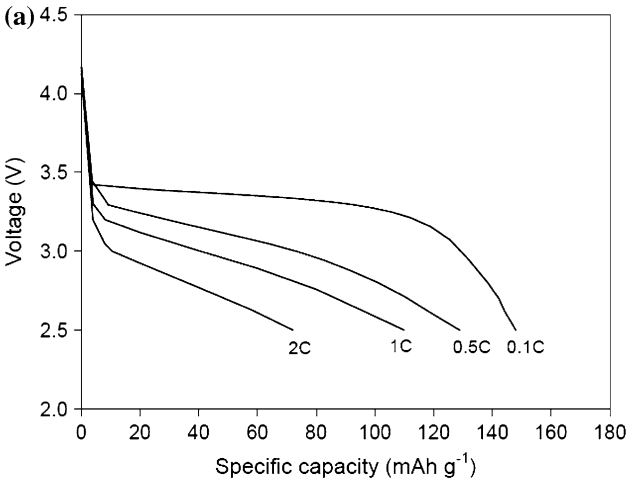

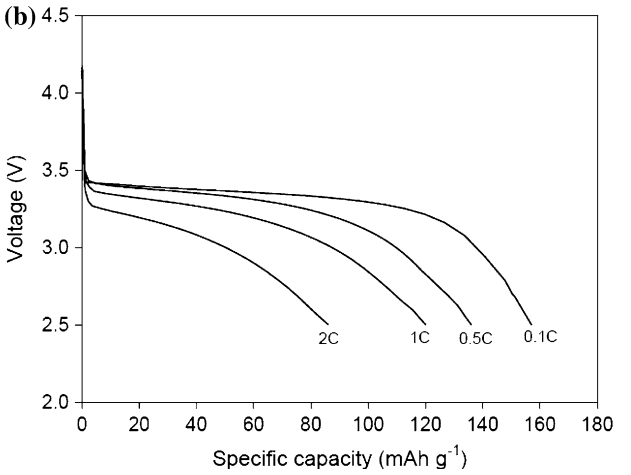

Fig. 8 Discharge curves of $LiFePO_4$/C powder (**a**) and $LiFe_{0.9}Mg_{0.1}PO_4$/C powder (**b**) at different current. The electrode was charged up to 4.2 V at 0.1 C prior to each discharge at various rates

electrode was charged up to 4.2 V at 0.1 C prior to each discharge. The $LiFePO_4$/C and $LiFe_{0.9}Mg_{0.1}PO_4$/C showed good rate capabilities, and the discharge capacities at 1 C were 110 and 120 mAh g^{-1}, respectively. The $LiFe_{0.9}Mg_{0.1}PO_4$/C has larger capacities compared with the $LiFePO_4$/C at all C-rates. The enhanced rate capability when the Mg-substituted for Fe in the precursor mixture is more likely to originate in the electronic conductivity. On the other hand, these good rate capabilities may attribute to the small particle size and enhanced the electronic conductivity of the $LiFePO_4$/C and $LiFe_{0.9}Mg_{0.1}PO_4$/C using carbon coating. In order to enhance the electronic conductivity of the material, extensive studies have been carried out by using some carbon coating techniques [2–7, 28]. Carbon coating on the particle is effective in decreasing the resistance of the cathode.

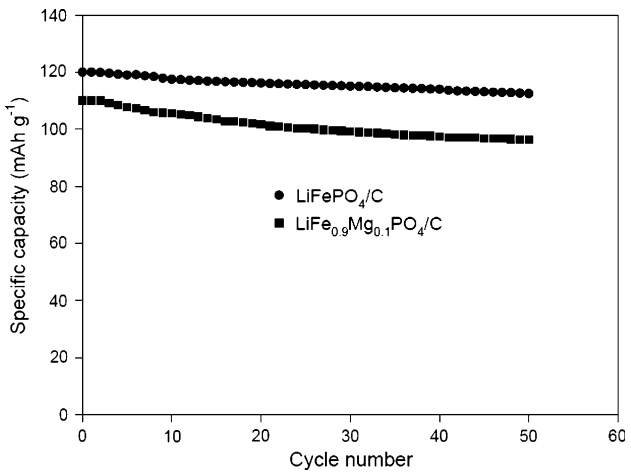

Fig. 9 Cycleability of Li–$LiFePO_4$/C and Li–$LiFe_{0.9}Mg_{0.1}PO_4$/C coin cells at 1 C

Figure 9 shows the specific capacity of the $LiFePO_4$/C and $LiFe_{0.9}Mg_{0.1}PO_4$/C in function of the cycle number at 1 C. The initial discharge capacities of the $LiFePO_4$/C and $LiFe_{0.9}Mg_{0.1}PO_4$/C were 110 and 120 mAh g^{-1}, respectively. The capacity fading over 50 cycles is 12% for $LiFePO_4$/C, but only 6% for $LiFe_{0.9}Mg_{0.1}PO_4$/C. The good cycling performance of the $LiFe_{0.9}Mg_{0.1}PO_4$/C is attributed to the enhancement of the electronic conductivity by the Mg substitution.

4 Conclusions

The spherical $LiFePO_4$/C and $LiFe_{0.9}Mg_{0.1}PO_4$/C powders have been synthesized via a uniform-phase precipitation method. The uniform spherical particles as prepared are amorphous, but they were crystallized to $FePO_4$ after calcining above 400 °C. After calcinations of it with LiOH and sugar or LiOH, $Mg(OH)_2$, and sugar, the final products, $LiFePO_4$/C, and $LiFe_{0.9}Mg_{0.1}PO_4$/C, became much denser, leading to the tap-density is as high as 1.75 g cm^{-3} for $LiFePO_4$/C and 1.77 g cm^{-3} for $LiFe_{0.9}Mg_{0.1}PO_4$/C, respectively. The excellent specific capacities of 148 and 157 mAh g^{-1} at 0.1 C were achieved for the $LiFePO_4$/C and $LiFe_{0.9}Mg_{0.1}PO_4$/C, respectively. Comparison of the cyclic voltammograms of $LiFePO_4$/C and $LiFe_{0.9}Mg_{0.1}PO_4$/C shows enhanced redox current and reversibility for the sample substituting Mg on the Fe site. $LiFe_{0.9}Mg_{0.1}PO_4$/C exhibits good high-rate and cycle performances. This uniform-phase precipitation synthesis is an excellent powder preparation alternative method for high capacity cathode materials to be used in a Li-ion secondary battery.

References

1. Padhi AK, Nanjundaswamy KS, Goodenough JB (1997) J Electrochem Soc 144:1188
2. Yamada A, Chung SC, Hinokuma K (2001) J Electrochem Soc 148:A224
3. Ravet N, Chouinard Y, Magnan JF, Besner S, Gauthier M, Armand M (2001) J Power Sources 97/98:503
4. Huang H, Yin SC, Nazar LF (2001) Electrochem Solid-State Lett 4:A170
5. Chen Z, Dahn JR (2002) J Electrochem Soc 149:A1184
6. Hu Y, Doeff MM, Kostecki R, Fiñones R (2004) J Electrochem Soc 151:A1279
7. Belharouak I, Johnson C, Amine K (2005) Electrochem Commun 7:983
8. Chung SY, Blocking JT, Chiang YM (2002) Nat Mater 1:123
9. Yamada A, Yonemura M, Takei Y, Sonoyama N, Kanno R (2005) Electrochem Solid-State Lett 8:A55
10. Sun YK, Bae YC, Myung ST (2005) J Appl Electrochem 35:151
11. Ying J, Jiang C, Wan C (2004) J Power Sources 129:264
12. Ying J, Lei M, Jiang C, Wan C, He X, Li J, Wang L, Ren J (2006) J Power Sources 158:543
13. He P, Wang H, Qi L, Osaka T (2006) J Power Sources 158:529
14. Shi SQ, Liu LJ, Ouyang CY, Wang DS, Wang Z, Chen L, Huang X (2003) Phys Rev B 68:195108
15. Liu H, Cao Q, Fu LJ, Li C, Wu YP, Wu HQ (2006) Electrochem Commun 8:1553
16. Zhang M, Jiao LF, Yuan HT, Wang YM, Guo J, Zhao M, Wang W, Zhou XD (2006) Solid State Ionics 177:3309
17. Barker J, Saidi MY, Swoyer JL (2003) Electrochem Solid-State Lett 6:A53
18. Wang GX, Bewlay S, Yao J, Ahn JH, Dou SX, Liu HK (2004) Electrochem Solid-State Lett 7:A503
19. Wang D, Li H, Shi S, Huang X, Chen L (2005) Electrochim Acta 50:2955
20. Hong J, Wang C, Kasavajjula U (2006) J Power Sources 162:1289
21. Wang C, Hong J (2007) Electrochem Solid-State Lett 10:A65
22. Wilhelmy RB, Matijević E (1987) Colloids Surf 22:111
23. Springsteen LL, Matijević E (1989) Colloid Polym Sci 267:1007
24. Kandori K, Nakashima H, Ishikawa T (1993) J Colloid Interface Sci 160:499
25. Kandori K, Kuwae T, Ishikawa T (2006) J Colloid Interface Sci 300:225
26. Scaccia S, Carewska M, Wisniewski P, Prosini PP (2003) Mater Res Bull 38:1155
27. Wang YQ, Wang JL, Yang J, Nuli JN (2006) Adv Funct Mater 16:2135
28. Franger S, Cras FL, Bourbon C, Rouault H (2002) Electrochem Solid-State Lett 5:A231